Journal of Geodynamics 68 (2013) 29–36

Contents lists available at SciVerse ScienceDirect

Journal of Geodynamics

journal homepage: http://www.elsevier.com/locate/jog

Precise determination of ocean tide loading gravity effect for absolute gravity stations in coastal area of China: Effects of land–sea boundary and station coordinate

Jiangcun Zhou[a,*], Cheinway Hwang[b], Heping Sun[a], Jianqiao Xu[a], Weimin Zhang[a,c], Ricky Kao[d], Tze-Chiang Cheng[b]

[a] State Key Laboratory of Geodesy and Earth's Dynamics, Institute of Geodesy and Geophysics, Chinese Academy of Sciences, Wuhan 430077, China
[b] Department of Civil Engineering, National Chiao Tung University, 1001 Ta Hsueh Road, Hsinchu 300, Taiwan, ROC
[c] National Geodetic Observatory, Institute of Geodesy and Geophysics, Chinese Academy of Sciences, Wuhan 430077, China
[d] Department of Geomatics Engineering, University of Calgary, 2500 University Drive NW, Calgary, AB, Canada T2N 1N4

ARTICLE INFO

Article history:
Received 30 October 2012
Received in revised form 12 March 2013
Accepted 12 March 2013
Available online 21 March 2013

Keywords:
Absolute gravity
Integrated Green's function
Land–sea boundary
Ocean tide loading
Tide gauge record

ABSTRACT

Gravity effect due to ocean tide loading (OTL) is an important signal and correction in various gravimetric applications. In this paper, we assessed the OTL gravity effects at four absolute gravity (AG) stations in coastal China from several perspectives. The integrated Green's function of the Newtonian part was derived analytically and that of the elastic part was computed based on the PREM earth model. Ocean tide (OT) records near the four AG stations were used to enhance the accuracy of the global ocean tide model of NAO99b and the regional model of NAO99jb for the innermost field (<0.02°). The high-resolution digital elevation model (DEM) from the Shuttle Radar Topography Mission (SRTM) was used to define the land–sea boundary in the optimized near field (<1.0°). Results show that the high-resolution land–sea boundary is indispensible for OTL gravity modeling when the shoreline near a coastal station is complex. The SRTM-based OTL model outperforms the GMT-based model shoreline in terms of the agreement between modeled and observed gravity residuals at the four stations. The final gravity residuals, corrected for OTL, at the four stations are significantly smaller than those without OTL corrections. We give examples of accuracy requirements in coordinates at Qingdao for different station heights. At a station height of 80 m and to ensure a 0.1 μgal accuracy in OTL modeling, the required accuracies in the horizontal and vertical coordinate are 2.5 and 1. 3 m, respectively. For a new coastal station and an expected OTL accuracy, one should inspect the variation of OTL due to coordinate variation to find a best strategy to determine the required accuracy of coordinate.

1. Introduction

Ocean tide loading (OTL) is caused by the ocean tide-induced mass redistribution. OTL gives rise to gravity change and surface deformation, which are increasingly important for investigations of many geodetic and geophysical problems. For example, OTL gravity effect should be removed from observed gravity tidal parameters to set up a gravity reference (Hsu et al., 2000), to detect the translational oscillation of the Earth's inner core (Courtier et al., 2000; Sun et al., 2004; Xu et al., 2010), to evaluate the eigen-period of the Earth's free core nutation (Sun et al., 2002, 2003; Xu et al., 2004; Ducarme et al., 2007), and consequently to evaluate the viscosities of the core-mantle boundary (Sun et al., 2009; Cui et al., 2012). Some of these applications use gravity data from a global network of superconducting gravimeters, under the Global Geodynamics Project (GGP; Crossley et al., 1999). Many of the GGP stations, e.g., Syowa, Hsinchu and Concepcion, are located in coastal areas. In addition, absolute gravimetry has become increasingly an effective tool in monitoring phenomena ranging from sea level change to mass transfer of geodynamic origins (Larson and van Dam, 2000; van Dam et al., 2000; Lysaker et al., 2008; Llubes et al., 2008). Many such measurements are made in coastal zones.

It is widely known that OTL gravity effect in a coastal zone is more difficult to model in comparison to inland areas. In general, the OTL gravity effect will decrease with increasing distance from the ocean. In order to adequately utilize gravity observations in a coastal zone, OTL gravity effects must be modeled with a great care. According to the theory of OTL (Longman, 1962, 1963; Farrell, 1972; Goad, 1980; Agnew, 1997), Green's function and ocean tide are two dominating factors for OTL modeling. Green's function is based on

* Corresponding author. Tel.: +86 15071302635.
E-mail address: zjc@asch.whigg.ac.cn (J. Zhou).

0264-3707/$ – see front matter © 2013 Elsevier Ltd. All rights reserved.
http://dx.doi.org/10.1016/j.jog.2013.03.003

the earth model (Farrell, 1972; Pagiatakis, 1990; Wang et al., 1996). Ocean tide for OTL computation is mostly based on a combination of global and a regional tide model, but there have been attempts to enhance OTL accuracy by direct use of tidal records near gravity stations (Neumeyer et al., 2005; Sun et al., 2006; Lysaker et al., 2008).

In addition to Green's function and ocean tide, the land–sea boundary also plays an important role in OTL modeling (Bos et al., 2002; Bos and Baker, 2005; Lysaker et al., 2008). The coastline dataset of Wessel and Smith (1996) is widely used in many OTL programs to define the land–sea boundary (Agnew, 1997; Matsumoto et al., 2001; Bos and Baker, 2005; Scherneck and Bos, 2006). With a spatial resolution up to 90 m, the SRTM DEM is believed to better define the land–sea boundary than the coastline dataset of Wessel and Smith (1996). Several other factors also contribute to OTL accuracy when a gravity station is very close to sea (within several hundreds of meter). For example, Bos et al. (2002) and Hwang and Huang (2012) showed that the OTL gravity effect also depends on the height of a gravity station sufficiently close to sea. Also, for a coastal station, it is not clear how the horizontal coordinate accuracy will affect the OTL accuracy.

With the above background, the objective of this paper is to assess the sensitivities of land–sea boundary and station coordinates on OTL model accuracy. Absolute gravity data and tide gauge records collected at four coastal stations along the coastal area of China will be used in these investigations.

2. Time- and frequency-domain modeling of OTL gravity effect

According to the theory of Farrell (1972), the OTL gravity effect, L, can be expressed by the convolution

$$L(\theta, \lambda, t) = R^2 \rho \int_0^{2\pi} \int_0^{\pi} H(\psi, \alpha, t) G(\psi) \sin\psi d\psi d\alpha \quad (1)$$

where θ and λ are co-latitude and longitude of the location of interest, respectively, t is time. R is the mean radius of the Earth (about 6371 km), ρ is the density of sea water (about 1025 kg/m^3), H is the instantaneous tidal height at t, ψ and α are the spherical distance and azimuth between the location and differential spherical surface area ($\sin\psi\, d\psi\, d\alpha$), and G is the Green's function for gravity effect. The two quantities ψ and α form the spherical surface coordinate system. The latest version of SPOTL uses a density model that accounts for the spatial variation of sea water density (Agnew, 2012).

The tidal height can be expanded into a series of harmonic functions with known tidal frequencies. Hence, we can compute OTL for each constituent (harmonic) with known frequency and omit the time dependence. For example, Goad (1980) used the integrated Green's function method for numerical convolution based on Eq. (1). Other examples are SPOTL developed by Agnew (1997) and SGOTL developed by Hwang and Huang (2012). In the frequency domain, Eq. (1) can be numerically implemented by

$$\begin{pmatrix} L_\omega \cos\varphi_\omega \\ L_\omega \sin\varphi_\omega \end{pmatrix} = \rho \sum_i \sum_j \begin{pmatrix} H_\omega \cos\phi_\omega \\ H_\omega \sin\phi_\omega \end{pmatrix} I(\psi_i)\delta\alpha \quad (2)$$

where ω is a tidal frequency, L_ω and φ_ω are the amplitude and phase of OTL at ω, which are the functions of station coordinates (θ, λ). H_ω and ϕ_ω are the amplitude and phase of ocean tidal height at ω, which are the functions of tidal ocean mass coordinates (ψ, α), and

$$I(\psi_i) = R^2 \int_{\psi_i - \delta\psi/2}^{\psi_i + \delta\psi/2} G(\psi) \sin\psi d\psi \quad (3)$$

is the integrated Green's function (Goad, 1980; Agnew, 1997),$\delta\psi$ and $\delta\alpha$ are the step sizes of integrated Green's function and azimuth. In practice, the step size should be variable. In general, it increases with the increasing angular distance (Agnew, 1996).

The Green's function for the OTL gravity effect consists of two parts, i.e., the Newtonian part and the elastic part. The integrated Green's function for Newtonian part can be derived according to Agnew (2012). Neglecting station height, the formula of Green's function for the elastic part is

$$G^E(\psi) = \frac{f}{R^2} \sum_{n=0}^{\infty} \{(n+1)k'_n - 2h'_n\} P_n(\cos\psi) \quad (4)$$

where h'_n and k'_n are load Love numbers and P_n is the Legendre polynomial, and n is the degree. The derivation of the integrated Green's function of the elastic part involves an infinite series of the integral of the Legendre polynomial. According to the recursive formula of the Legendre polynomial (Heiskanen and Moritz, 1985), the integral of the Legendre polynomial is

$$\int_{\psi-\delta/2}^{\psi+\delta/2} P_n(\cos\psi)\sin\psi d\psi = -\int_{\cos(\psi-\delta/2)}^{\cos(\psi+\delta/2)} P_n(x)dx = \frac{P_{n+1}(x) - P_{n-1}(x)}{2n+1} \Bigg|_{\cos(\psi+\delta/2)}^{\cos(\psi-\delta/2)} \quad (5)$$

Eq. (5) shows that the integral of the Legendre polynomial decreases as $1/n$. Therefore, the infinite series of integrated Legendre polynomial converges faster than that of Legendre polynomial and can be truncated beyond a certain degree under a desired numerical accuracy.

In this paper, Eq. (3) is first used to compute the integrated Green's function and then Eq. (2) is used to calculate OTL for selected leading constituents (each with a frequency), and finally the OTL effect at any time t due to the leading constituents is computed as

$$g(t) = \sum_\omega L_\omega \times \cos[\omega(t - t_0) + \chi_\omega - \varphi_\omega] \quad (6)$$

where the sum is over the leading constituents, and χ_ω is the astronomic argument of that constituent with respect to a reference time t_0. This is the OTL effect in the frequency domain.

If a regional ocean tide model is available, it should be used to enhance the OTL modeling. If a gravity station is near the sea, incorporating nearby tidal records will also improve the OTL model accuracy (Neumeyer et al., 2005; Sun et al., 2006; Lysaker et al., 2008). Because the gravity stations in this paper are all near the sea, we use the tide gauge record as the mean value in a circle with a radius of 0.02° (the innermost field) centered at the stations for each epoch to improve the ocean tide models. Because the ocean tide records (parallel with the gravity records) in this paper are given in the time domain and are not long enough to extract the harmonic constants, we carried out the OTL computation in the time and frequency domains using the following steps:

(a) Calculate the OTL effect by considering the integration area of $0.02 \le \psi \le 180°$ and $0 \le \alpha \le 360°$. In the integral, the step $\delta\psi$ increases with ψ. Table 1 shows $\delta\psi$ with respect to ψ. The step of azimuth remains unchanged for all ψ. In this step the integration is divided into the integrations over the near field ($0.02 \le \psi \le 1°$) and the far field ($1 \le \psi \le 180°$), and the land–sea boundaries for these two fields are different, but are optimized (see Section 4).
(b) Within the innermost field ($\psi \le 0.02°$), calculate the transfer coefficient, C, from tidal height to OTL gravity effect by setting

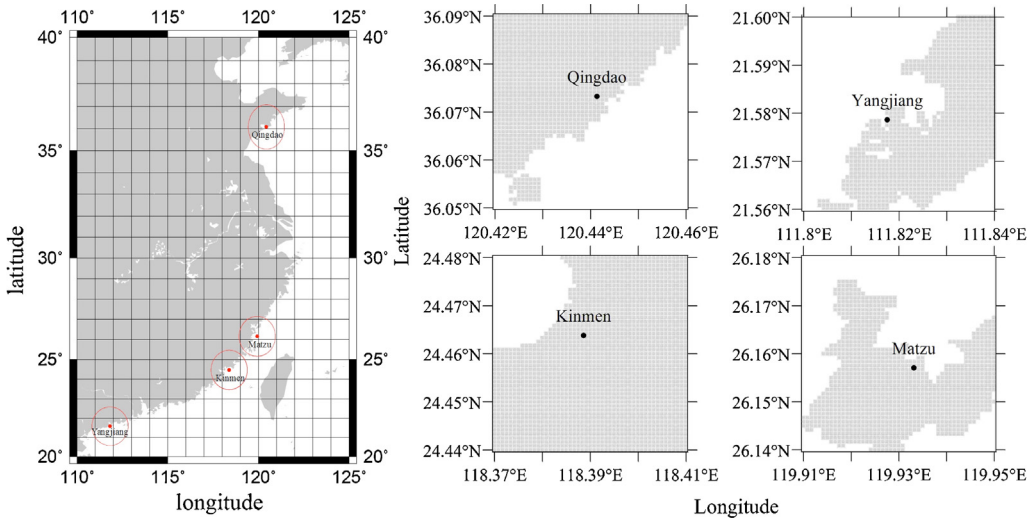

Fig. 1. Distribution of four absolute gravity stations. Solid dots show the stations and the circles the integration areas in a radius of 1.0° (near field) centered at the stations; the right panel shows the detailed land coverages (shaded areas) near stations.

tidal height as 1 m (unit tidal height). The innermost field is centered at the station, i.e.

$$C(\theta,\lambda) = R^2\rho \int_0^{2\pi}\int_0^{0.02} \Theta(\psi,\alpha)G(\psi)\sin\psi d\psi d\alpha \qquad (7)$$

where Θ is the ocean function, which is defined by land–sea boundary. In Eq. (7), the instantaneous tidal height is equivalent to the ocean function and the integral steps are the same as the ones in the ψ band from 0.02° to 1.0° in Table 1. In fact, C is the gravity change per unit tidal height (1 m).

(c) Combine the above two results to obtain the final OTL gravity by

$$g'(t) = g(t) + C \times O(t) \qquad (8)$$

where $O(t)$ is the ocean tide record from tide gauge in meter.

3. Data descriptions

3.1. Absolute gravity data

Absolute gravity surveys were conducted using two FG5 gravimeters at four stations in coastal areas of China (Fig. 1) in different years. The absolute gravity data were collected as follows. For each station, we collected about 100 drops in a set of 30 min, and these 100 values were averaged to form a mean gravity of this set. For all four stations, we collected 24 h of data in 48 sets (Table 2). The gravity observations were corrected for the solid earth tides by the Earth tide model of Dehant et al. (1999) and tide generating potential expansion of Xi (1989). Corrections due to speed of light, local air pressure, and polar motion (Wahr, 1985) were also carried out to obtain the gravity residuals which contain mainly the OTL gravity effect.

Table 1
Step sizes for numerical convolution.

ψ	$\delta\psi$	$\delta\alpha$
0.02°–1.0°	0.001°	0.5°
1°–10°	0.1°	0.5°
10°–90°	0.5°	0.5°
90°–180°	1.0°	0.5°

3.2. Earth models and ocean tide models

From Eq. (1), Green's function and tidal height are two important quantities in the computation of OTL gravity effect. These two quantities are determined by the Earth model and ocean tide model, respectively. For OTL modeling, a spherical symmetric model such as the SNREI (Spherical Non-Rotational Elastic Isotropic) Earth is suitable. In this paper, we used the integrated Green's functions derived from the PREM model (Dziewonski and Anderson, 1981). Fig. 2 shows the elastic parts of the two integrated Green's functions for angular distances less than 1° by using the PREM model and the Gutenberg–Bullen A model used by Agnew (1997). The difference between them reaches about 25% for small angular distances, and the two are almost identical for larger angular distances. Therefore, at a coastal station, the elastic part of OTL is very sensitive to the adopted earth model. However, because the Newtonian part is much larger than elastic part (see the comparison in Fig. 8(d) later) at a coastal station, the total OTL effect (Newtonian plus elastic parts) based on these two integrated Green's functions will differ slightly.

The global and regional ocean tide models NAO99b as well as NAO99jb, developed by Matsumoto et al. (2000), were adopted for the OTL modeling in this paper. NAO99b and NAO99jb have a nominal spatial resolution of 0.5° and 5′, respectively. The short-period

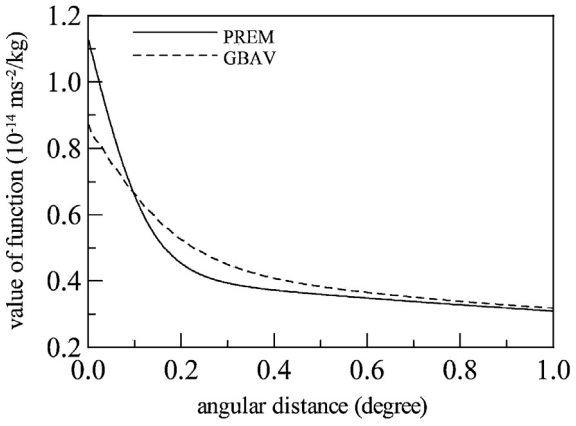

Fig. 2. Integrated Green's functions (elastic parts) based on the PREM and GBAV earth models. Note the large difference when the angular distance is small.

Table 2
Information about absolute gravity observations at four stations.

Station	Qingdao	Yangjiang	Kinmen	Matzu
Latitude (°)	36.07328	21.57861	24.46382	26.15708
Longitude (°)	120.44130	111.81750	118.38857	119.93315
Height (m)	30.90	38.00	35.74	42.43
Distance to coast (m)	370	60	590	90
Start time[a]	2003/04/18,06:08:15	2003/04/03,12:08:15	2005/02/21,02:08:31	2005/01/26,01:08:08
End time[a]	2003/04/19,05:38:15	2003/04/04,11:38:15	2005/02/22,01:37:58	2005/01/27,00:38:07

[a] Year/month/day, hour:minute:second.

constituents of NAO99b assimilated 5 years of T/P altimetry data into a hydrodynamic model with a spatial resolution of 0.5°, while NAO99b's long-period constituents are purely based on the solutions of the hydrodynamic equations without T/P data. Matsumoto et al. (2000) also optimized NAO99b over shallow waters by assimilation with tide gauge data. The tests with tide gauge data over shallow water areas by Matsumoto et al. (2000) showed that NAO99b performs better than the models of CSR4.0 (Eanes and Bettadpur, 1995; Eanes, 2002) and GOT99.2b (Ray, 1999) in the western Pacific that covers that area given in Fig. 1. Sun et al. (2005) also pointed out that NAO99b performs better in china area such as at Wuhan station. Additionally, coastal tide gauge data were assimilated in the regional model NAO99jb.

Importantly, there are in total 16 diurnal and semidiurnal constituents ($Q_1, O_1, M_1, P_1, K_1, J_1$,$Oo_1$, $2N_2$, μ_2, N_2, ν_2, M_2, L_2, T_2, S_2 and K_2) in NAO99b and NAO99jb. This is also why we used them in our computation. Because the lengths of gravity records in this paper were about one day, the long-term ocean tides were ignored. In addition, we collected ocean tide records parallel in time with the gravity observations near the four gravity stations for use in Eq. (8). Fig. 3 shows the tidal records near the four gravity stations. The tide gauges are within few hundreds of meter to the gravity stations. The tidal variations were dominated by the semidiurnal components. During the measuring campaigns, the largest tidal range is found at Matzu and is about 5 m. The large tide at Matzu is mainly caused by the complex shoreline here and the amplifying effect from the Taiwan Strait. Located in the south China sea, Yangjiang has the least tidal range. We expect the largest OTL gravity effect at Matzu and the least at Yangjiang.

3.3. Land–sea boundaries

In addition to the Green's function and tidal heights, the actual coverage of the sea that is used for numerical convolution is also an important factor, and is determined by the land–sea boundary. Two such boundaries were used in this paper. For the near field, which was defined as the area within a 1.0°-circle centered at given gravity station (see also Section 2), the SRTM DEM was used to define the land–sea boundary. The SRTM DEM has a nominal resolution of 90 m (Farr and Kobrick, 2000; Farr et al., 2007). The reason of the choice of a 1.0°-circle will be given in Section 4.1; For the far field, which is outside of this 1.0°-circle, the land–sea boundary was defined by the shoreline data in the program SPOTL (Agnew, 1996), which has a nominal spatial resolution of about 1.7 km and is based on GMT's shoreline (Wessel and Smith, 1996).

4. Results and discussions

4.1. Optimal radius for using high-resolution shoreline

Because the near field effect dominates the OTL result, this effect must be precisely modeled and is now discussed in detail. As mentioned in Section 1, not only a local ocean tide model and tide gauge records are important for precise OTL modeling, but also a high-resolution shoreline. Within the near field, a high-resolution shoreline should be used, and a coarser shoreline can be used in the far field. Also, the steps of integral can be larger in the far field. Here we conduct a numerical test to define the far field. We experiment with only the M_2 constituent of NAO99b as follows:

(a) Choose a circle with a radius of 1.5° within which a high-resolution shoreline is taken into account, and calculate the OTL gravity (denoted as V_1).

(b) Choose any a circle whose radius <1.5° and calculate the OTL gravity effect (denoted as V_2).

(c) Calculate the difference percentage using $(V_2 - V_1)/V_1 \times 100\%$.

(d) Repeat (b) and (c) for various radii to decide the optimal radius.

The result from Step (a) is considered as the "true" OTL effect because 1.5° is considered to be sufficiently large. Fig. 4 shows the difference percentages for various radii. In Fig. 4, the percentages are all below 0.5% (in absolute values). At the four gravity stations, the 1.0°- and 0.5°-radii result in difference percentages less than 0.05% and 0.1%, respectively. These differences are far below

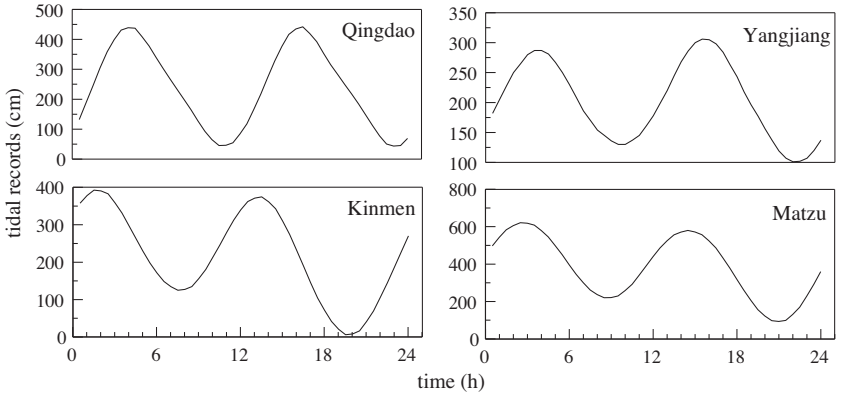

Fig. 3. One-day tidal records at four tide gauges near the gravity stations (the first samples correspond to the start times in Table 2).

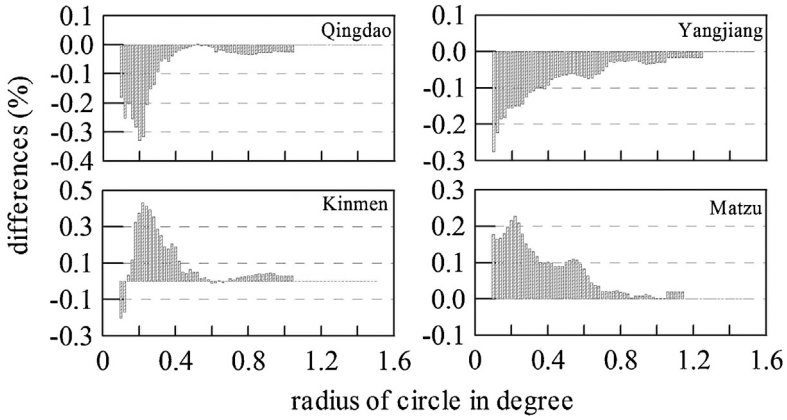

Fig. 4. The difference percentage (in %) as a function of the radius of circle (less than 1.5°) at the four gravity stations.

the current computational precision of OTL gravity effect (Bos and Baker, 2005). It is noted that, if the high-resolution shoreline is not used in the case of 1.0° radius, the difference percentages reach 13%, 43%, 12% and 60% at Qingdao, Yangjiang, Kinmen and Matzu, respectively. This highlights the importance of a high-resolution shoreline for precise OTL modeling over coastal areas. Based on this numerical test, we adopt 1.0° as the optimal radius considering the computational efficiency and accuracy for the near field.

4.2. Effect of resolution of land–sea boundary

In theory, the accuracy of modeled OTL gravity effect increases with the resolution of land–sea boundary. To assess the land–sea effect, we calculated the OTL gravity by using different land–sea boundaries. In addition to the land–sea boundary based on the SRTM DEM, five land–sea boundaries from the GMT shoreline database (Wessel and Smith, 1996) were used for comparison. Because the SRTM land–sea boundary has a nominal 3″ resolution, we established five land–sea boundaries on a 3″ × 3″ grid from the full, high, intermediate, low and crude shorelines of GMT.

Fig. 5 shows the modeled hourly OTL gravity values using the six boundaries. In Fig. 5, the full resolution shoreline is denoted as GMTF (here F means "full"), and this is applied to other four cases. In general, the results from using the GMTC shoreline differ substantially from other results, so this shoreline set is not recommended for OTL modeling. At Qingdao and Kinmen, the results from the other five land–sea boundaries (i.e., excluding the GMTC shoreline) are nearly the same. However, at Yangjiang and Matzu, the results are highly dependent on the boundary used. A plausible explanation is that at Yangjiang and Matzu the shoreline geometries are very complicated compared to Qingdao and Kinmen (Fig. 1) and these two stations are closer to the ocean. The result in Fig. 5 suggests that a high-resolution land–sea boundary is critical to the precision modeling of OTL gravity effect over an area surrounded by a complex shoreline.

4.3. Effect of OTL correction on AG gravity residual

The gravity variations at the four stations after the corrections made in Section 3.1 are largely due to OTL. Therefore, such variations can be further reduced by applying OTL corrections. This results in the final gravity residuals. One indicator for the accuracy of an OTL gravity model is the standard deviation of the final gravity residuals. A small standard deviation suggests a good OTL modeling and vice versa. Fig. 6 shows the standard deviations of the residual gravity values with and without OTL corrections. It is clear that the standard deviations decrease notably after applying the OTL corrections. In particular, the decrease is pronounced at stations with large tidal amplitudes. For example, the standard deviation of the raw gravity residual (labeled by RAW) at Matzu is 14.5 μgal (1 μgal = 10^{-8} m/s^2), which is reduced to about 4.0 μgal after the OTL correction using the SRTM land–sea boundary for the near field (labeled by SRTM).

Fig. 6 suggests that the SRTM-based boundary produces the smallest standard deviations, or the best OTL model values. At Yangjiang and Matzu, the final gravity residuals are much smaller than the values without OTL corrections. At Qingdao and Kinmen, the reduction of gravity residuals due to OTL corrections is also significant, but the extent of reduction is not as large as the cases at

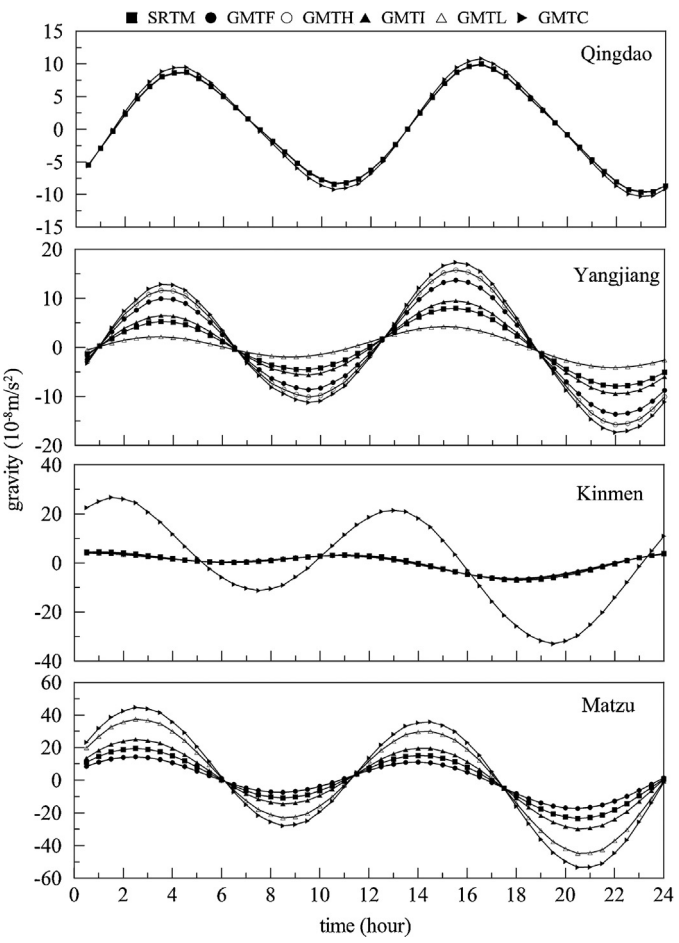

Fig. 5. The modeled hourly OTL gravity values with different land–sea boundaries.

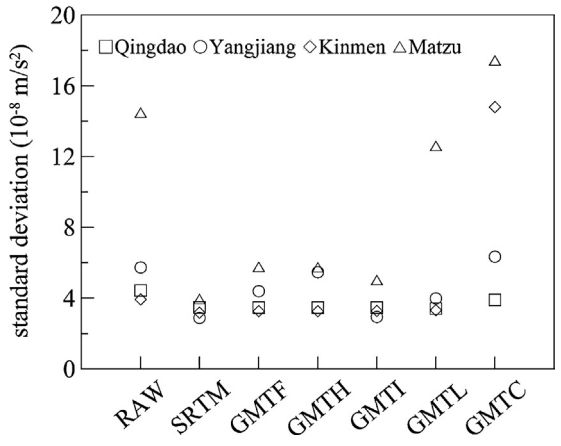

Fig. 6. Standard deviations of the gravity residuals before and after OTL corrections. RAW corresponds to the values of gravity residuals and the others to those of final gravity residuals.

Yangjiang and Matzu. Note that, the conclusion about the SRTM-based boundary is shown to be valid for the four stations in this paper, but may not be valid elsewhere. In some cases, the use of a GMT boundary other than GMTC can lead to a good OTL result. For example, with GMTI and GMTL at the stations other than Matzu, good OTL results are achieved. GMTH performs very well at Qingdao and Kinmen. This shows that the accuracy of GMT boundary is station-dependent. This is due to the unevenly distributed data used to construct the land–sea boundary of GMT (Wessel and Smith, 1996).

Fig. 7 compares the observed and modeled OTL gravity effects. Fig. 7 shows evident semidiurnal gravity variations due to M_2, accompanied by variations of non-tidal origins. It is noted that these non-tidal variations were not excluded in the computation of the standard deviations of the gravity residuals and the final gravity residuals. In fact, these non-tidal gravity variations have contributed to the standard deviations given in Fig. 6. These anomalies are likely to be caused by ocean waves. In conclusions, the OTL model with the SRTM land–sea boundary has delivered a promising result at the four coastal gravity stations, and the SRTM-based model is the best compared to the non-SRTM based models.

4.4. Sensitivity of OTL to station coordinates

Here we investigate the effect of coordinate error on OTL model error near coasts. As an example, Fig. 8(a) and (b) shows the amplitude of the M_2 OTL gravity effect (in μgal) around Qingdao station for station heights of 10 and 80 m, respectively. The OTL amplitude increases rapidly with the station height, especially for the area at immediate vicinity of sea. Both cases show increasing gradients of OTL towards the ocean, suggesting that, as the station gets closer to the coast, the requirement of precise coordinates is increasingly demanding. At the station height of 10 m (Fig. 8(a)), the horizontal OTL gravity gradient towards the ocean is about 0.005 μgal/m at Qingdao. Here, to ensure a 0.1 μgal accuracy for the modeled OTL gravity (0.1 μgal is 1/10 of current best accuracy from absolute gravity measurements, taking into account all instrument and correction errors), the accuracy for the horizontal coordinates should be about 20 m. At 80 m, the gradient at Qingdao station is about 0.04 μgal/m, requiring a horizontal coordinate accuracy of 2.5 m. The required accuracy will become more stringent as the station gets closer to the ocean. From Fig. 8(c), the M_2 amplitude increases almost linearly with the station height of the gravity station when the height is below 80 m. The amplitudes vary from 2 μgal to 8 μgal when the station height increases from 0 to 80 m. This corresponds to a vertical gravity gradient of about 0.075 μgal/m, demanding an accuracy of 1.3 m in the vertical coordinate. Thus, in a coastal area, the OTL gravity effect is very sensitive to the station height. Fig. 8(d) shows the integrated Green's functions of the Newtonian part at different station heights. The correspondence between integrated Green's function and station height in Fig. 8(d) is similar to that given by Bos et al. (2002). The effect of station height on OTL is significant when the spherical distance between the station and the nearest shoreline is smaller than 1.0°, and it is negligible when the spherical distance is much larger than 1.0°.

In conclusions, in OTL modeling the required accuracies for the horizontal and vertical coordinates increase with decreasing distance between the station and the oceans. Such requirements can be easily met using contemporary geodetic techniques such as Global Positioning System (GPS) and precision leveling. In a typical field work, a GPS station may be installed at a location few m away from the AG station. For coastal gravity stations like the ones in this paper, it is important to reduce the coordinates of the GPS station to the coordinates of the AG station to the same level of accuracies required by OTL modeling. Note that the required station coordinate accuracies here are specifically for station Qingdao only. For a new coastal absolute gravity station, we recommend that, users of gravity values collected here should (1) set the accuracy requirement for OTL correction, and (2) inspect the variation of OTL due to coordinate variation at the station, as in this paper, to determine the required

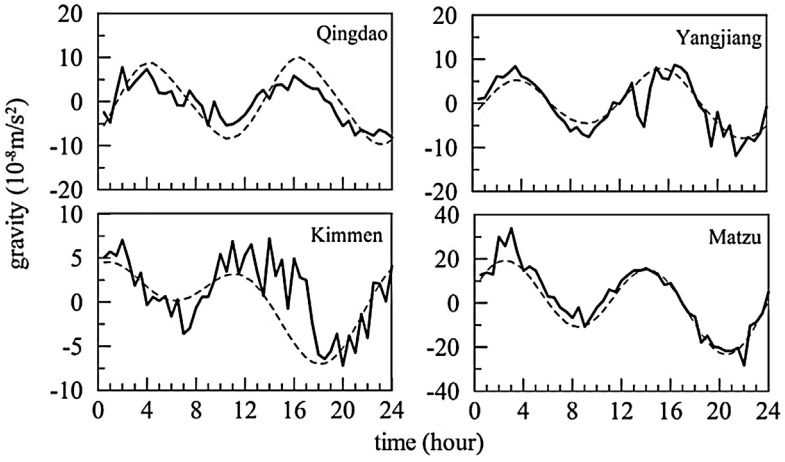

Fig. 7. Comparison between observed residual gravity values (solid lines, without OTL corrections) and modeled OTL gravity effects (dashed lines).

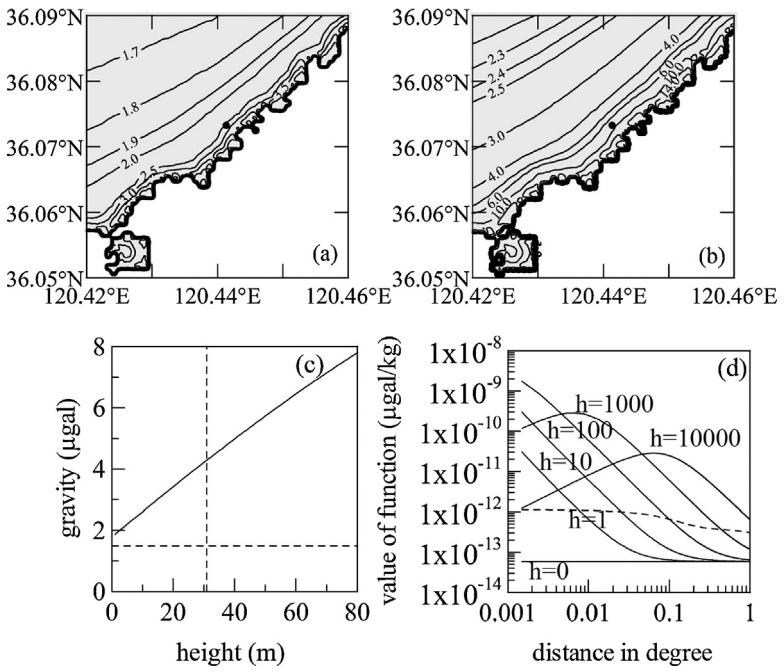

Fig. 8. (a) The amplitude of the M_2 OTL gravity effects (in μgal) around Qingdao station (solid dot) for station heights of 10 m; (b) the same as (a) but for station heights of 80 m; (c) the solid line shows the values at Qingdao varying with different heights and the horizontal dashed line shows the elastic part of OTL; the intersection of solid line and vertical dashed line shows the value for Qingdao station. (d) The Newtonian part of integrated Green's functions for different heights in m, the dashed line shows the elastic part of the integrated Green's function.

accuracy of coordinate that can meet the OTL accuracy requirement.

5. Conclusions

In this paper, we present a combined time and frequency domain approach for the modeling of OTL gravity effect at four coastal stations of China. In the OTL modeling, we divided the ocean tide contributions into three parts as the three fields: an innermost field (distance < 0.02° to the gravity station), the near field and the far field. In the innermost field, the OTL gravity effect was estimated by scaling the tidal height by a transfer coefficient obtained from the ocean function. In the near field, an optimal radius of 1.0° was determined and here we used a high-resolution land–sea boundary for the convolution of tidal heights with the Green's function. In the far field, a coarser land–sea boundary was used. Two earth models ware used for computing the elastic part of the Green's function. The difference between the two Green's functions reaches about 25% for small angular distances. But this difference results in a minor difference in the total OTL effect because the Newtonian part is dominant at a coastal station.

As a case study, the modeled OTL gravity effects at four coastal stations in China coast were assessed by gravity measurements collected by two absolute gravimeters. Six sets of land–sea boundary were used for the OTL modeling. The SRTM-based OTL model outperforms the GMT-based models in resolving the fine gravity effect of ocean tide loading in the near field. The results from using the GMT coarse shoreline differ substantially from other cases, so this shoreline set is not recommended for OTL modeling. The experience at Yangjiang and Matzu shows that, at a gravity station with large tidal amplitude and complicated shoreline geometry, the use of a high-resolution land–sea boundary is critical to the modeling accuracy. Therefore, one should carefully inspect the shoreline complexity near a given station to decide whether a high resolution land–sea boundary is necessary. At a coastal station, the station coordinate accuracy is also of great importance for OTL modeling accuracy. A case study at Qingdao with a station height of 80 m, the required accuracies in the horizontal and vertical coordinates are 2.5 and 1.3 m, respectively. Such coordinate accuracies can be easily achieved by contemporary geodetic techniques. Therefore, stations coordinates based on a map or a navigation-type GPS receiver will not be acceptable for the coastal stations in this paper, and this may apply to other coastal stations in the world.

Acknowledgements

This study is supported by the CAS/SAFEA International Partnership Program for Creative Research Teams (Grant No. KZZD-EW-TZ-05) and the National Natural Science Foundation of China (Grant Nos. 41004009 and 41021003) and by the National Science Council of Taiwan (Grant no.: 101-2611-M-009-001). We thank DC Agnew for providing with the SPOTL software and shoreline databases.

References

Agnew, D.C., 1996. SPOTL: Some programs for ocean-tide loading. SIO Ref. Ser. 96-8, Scripps Institution of Oceanography, La Jolla, CA, 35 pp.
Agnew, D.C., 1997. A program for computing ocean tide loading. Journal of Geophysical Research 102 (B3), 5109–5110.
Agnew, D.C., 2012. SPOTL: Some programs for ocean-tide loading. Technical report. Scripps Institution of Oceanography, La Jolla, CA.
Bos, M.S., Baker, T.F., 2005. An estimate of the errors in gravity ocean tide loading computation. Journal of Geodesy 79 (1-3), 50–63.
Bos, M.S., Baker, T.F., Røthing, K., Plag, H.P., 2002. Testing ocean tide models in the Nordic seas with tidal gravity observations. Geophysical Journal International 150, 687–694.
Courtier, N., Ducarme, B., Goodkind, J., et al., 2000. Global superconducting gravimeter observations and the search for the translationalmodes of the inner core. Physics of the Earth and Planetary Interiors 117, 3–20.
Crossley, D., Hinderer, J., Casula, G., et al., 1999. Eos Transactions, American Geophysical Union 80 (11), 121125–121126.
Cui, X.M., Sun, H.P., Xu, J.Q., et al., 2012. Application of superconductive gravity technique on the constraints of core-mantle coupling parameters. Science China Earth Sciences, http://dx.doi.org/10.1007/s11430-011-4346-3.
Dehant, V., Defraigne, P., Wahr, J., 1999. Tides for a convective Earth. Journal of Geophysical Research 104 (B1), 1035–1058.
Ducarme, B., Sun, H.P., Xu, J.Q., 2007. Determination of the free core nutation period from tidal gravity observations of the GGP superconducting gravimeter network. Journal of Geodesy 81 (3), 179–187.

Dziewonski, A.M., Anderson, D.L., 1981. Preliminary reference earth model. Physics of the Earth and Planetary Interiors 25, 297–356.
Eanes, R., 2002. The CSR4.0 Global Ocean Tide Model, ftp://www.csr.utexas.edu/pub/tide
Eanes, R., Bettadpur, S., 1995. The CSR 3.0 Global Ocean Tide Model, Tech. Memo.CSR-TM-95-06, Cent. for Space Res. Univ. of Tex, Austin.
Farr, T.G., Kobrick, M., 2000. Shuttle radar topography mission produces a wealth of data. American Geophysics Union, Eos 81, 583–585.
Farr, t., Rosen, P., Caro, E., et al., 2007. The shuttle radar topography misson. Reviews of Geophysics 45, RG2044, http://dx.doi.org/10.1029/2005RG000183.
Farrell, W., 1972. Deformation of the Earth by surface loads. Reviews of Geophysics and Space Physics 10, 761–797.
Goad, C.C., 1980. Gravimetric tidal loading computed from integrated Green's function. Journal of Geophysical Research 85, 2679L 2683.
Heiskanen, W.A., Moritz, H., 1985. Physical Geodesy, Tech. University Graz, Reprint.
Hsu, H., Sun, H.P., Xu, J.Q., Tao, G.X., 2000. International tidal gravity reference values at Wuhan station. Science in China (Series D) 43 (1), 77–83.
Hwang, C., Huang, J.F., 2012. SGOTL: a computer program for modeling high-resolution, height-dependent gravity effect of ocean tide loading. Terrestrial Atmospheric and Oceanic Sciences 23, 219–229.
Larson, K., van Dam, T., 2000. Measuring postglacial rebound with GPS and absolute gravity. Geophysical Research Letters 27 (23), 3925–3928.
Llubes, M., Florsch, N., Boy, J.P., et al., 2008. Multi-technique monitoring of ocean tide loading in northern France. Comptes Rendus Geoscience 340 (6), 379–389.
Longman, I.M., 1962. A Green's function for determining the deformation of the earth under surface mass loads. 1. Theory. Journal of Geophysical Research 68 (2), 845–850.
Longman, I.M., 1963. A Green's function for determining the deformation of the earth under surface mass loads, 2, computation and numerical result. Journal of Geophysical Research 68 (2), 485–496.
Lysaker, D.I., Breili, K., Pettersen, B.R., 2008. The gravitational effect of ocean tide loading at high latitude coastal stations in Norway. Journal of Geodesy 82, 569–583.
Matsumoto, K., Sato, T., Takanezawa, T., et al., 2001. GOTIC2: a program for computation of oceanic tidal loading effect. Journal of Geodetic Society of Japan 47, 243–248.
Matsumoto, K., Takanezawa, T., Ooe, M., 2000. Ocean tide models developed by assimilating TOPEX/POSEIDON altimeter data into hydrodynamical model: a global model and a regional model around Japan. Journal of Oceanography 56, 567–581.
Neumeyer, J., del Pino, J., Dierks, O., et al., 2005. Improvement of ocean loading correction on gravity data with additional tide gauge measurements. Journal of Geodynamics 40, 104–111.
Pagiatakis, S.D., 1990. The response of a realistic earth to ocean tide loading. Geophysics Journal International 103 (2), 541–560.
Ray, R.D., 1999. A global ocean tide model from TOPEX/POSEIDON altimetry: GOT99. NASA Technical Memorandum 209478. Goddard Space Flight Centre, Greenbelt.
Scherneck, H. G., Bos, M., 2006. Ocean tide loading provider. http://www.oso.chalmers.se/∼loading/ Backup site at GEODAC: http://www.geodac.fc.up.pt/loading/
Sun, H.P., Cui, X.M., Xu, J.Q., Ducarme, B., Liu, M.B., Zhou, J.C., 2009. Preliminary application of superconductive gravity technique on the investigation of viscosity at core-mantle boundary. Chinese Journal of Geophysics 52, 311–321.
Sun, H.P., Ducarme, B., Xu, J.Q., 2002. Preliminary results of the free core nutation eigenperiod obtained by stacking SG observations at GGP stations. Bull D'informations de Marées Terrestres 136, 10725–10728.
Sun, H.P., Hsu, H., Chen, W., Chen, X.D., Zhou, J.C., Liu, M., Gao, Shan, 2006. Study of Earth's gravity tide and oceanic loading characteristics in Hong Kong area. Chinese Journal of Geophysics 49 (3), 724–734 (in Chinese).
Sun, H.P., Hsu, H.Z., Zhou, J.C., Chen, X.D., Xu, J.Q., Zhou, B.L., Hao, X.H., Liu, M., 2005. Latest observation results from superconducting gravimeter at station Wuhan and investigation of the ocean tide models. Chinese Journal of Geophysics: Chinese Edition 48 (2), 299–307.
Sun, H.P., Xu, J.Q., Ducarme, B., 2003. Experimental earth tidal models in considering nearly diurnal free wobble of the Earth's liquid core. Chinese Science Bulletin 48, 935–940.
Sun, H.P., Xu, J.Q., Ducarme, B., 2004. Detection of the Translational Oscillation of the Earth's Solid Inner Core Based on the International SG Observations. Chinese Science Bulletin 49 (11), 1165–1176.
van Dam, T., Larson, K.M., Wahr, J., Francis, O., Gross, S., 2000. Using GPS and gravity to infer ice mass changes in Greenland. EOS 81, 421–427.
Wahr, J.M., 1985. Deformation induced by polar motion. Journal of Geophysical Research 90 (B11), 9363–9368.
Wang, H., Hsu, H., Li, G., 1996. Improvement of computations of load Love numbers of SNREI earth model. Chinese Journal of Geophysics 39 (Suppl.), 182–189 (in Chinese).
Wessel, P., Smith, W.H.F., 1996. A global, self-consistent, hierarchical, high-resolution shoreline database. Journal of Geophysical Research 101 (B4), 8741–8743.
Xi, Q., 1989. The precision of the development of tidal generating potential and some explanatory notes. Bull D'informations de Marées Terrestres 105, 7396–7404.
Xu, J.Q., Sun, H.P., Ducarme, B., 2004. A global experimental model for gravity tides of the Earth. Journal of Geodynamics 38, 293–306.
Xu, J.Q., Sun, H.P., Zhou, J.C., 2010. Experimental detection of the inner core translational triplet. Chinese Science Bulletin 55 (3), 276–283.